

# APPLICATION OF TLS FOR CHANGE DETECTION IN ROCK FACES

M. Alba, F. Roncoroni, M. Scaioni

Politecnico di Milano, Dept. BEST, Polo Regionale di Lecco, via M. d'Oggiono 18/a, 23900 Lecco, Italy  
e-mail: {mario.alba, fabio.roncoroni, marco.scaioni}@polimi.it

Commission V, WG V/3

**KEY WORDS:** Change Detection, Deformation Monitoring, Natural Hazards, Rockfall, Terrestrial Laser Scanning

## ABSTRACT:

The paper describes some experiences carried out in monitoring of two rock faces in Italian Prealps in order to detect changes due to rock detachments. Since the forecasting of possible rockfall events is the main aim of this research, terrestrial laser scanning application was investigated for high precision deformation monitoring in this context. Firstly, problems concerning the data acquisition and the reduction of georeferencing errors are analyzed by comparing results obtained from different approaches. A method including the use of a removable steel pillar to constrain the 3D shifts of the instrumental reference system, and of ICP surface matching algorithm to solve for rotations gave the best results. Secondly, some techniques for filtering vegetation from point-clouds of cliffs are presented and discussed here. These are mainly based on 3D spatial filters. The use of an infrared camera integrated to terrestrial laser scanner is also proposed. Finally, results on the comparison of multi-temporal laser scans are presented, showing somehow the proposed pipeline can be successfully applied to detect small rock detachments of the size of a few cube centimetres.

## 1. INTRODUCTION

The problem of preventing or reducing damages of rockfalls is a challenging task, due to the very large number of feasible scenarios with the local morphology of the site providing an additional degree of freedom. Due to this complexity, several competences are needed to address at the best methods that have to be used in an integrated manner (Arosio *et al.*, 2009). In the scenario of technologies that can help to achieve this aim, *terrestrial laser scanning* (TLS) techniques have already proven the capability to provide useful data for geometric modeling of rock cliffs (Alba *et al.*, 2005) and for the geomorphological analysis (Roncella and Forlani, 2005; Abellán *et al.*, 2006). Today the interest of researchers is focusing on the application of TLS for monitoring with a twofold objective.

The first one concerns the understanding of ongoing millimetric deformations that can be a presignal of future failures. This task is really harsh, due to the need of measuring displacements that in many cases are lower than the uncertainty of TLS observations. In recent years, different *area-based deformation measurement* techniques have been applied to exploit the data redundancy achievable by laser scanning, in order to improve the precision (Lindenbergh and Pfeifer, 2005; Schneider, 2006). On the other hand, such methods require regular surfaces to be interpolated by analytical functions, at least at local level, and unfortunately this assumption rarely holds when dealing with rock cliffs.

Besides the problem of the required accuracy in data acquisition and modelling, varying from few cm to 0.1 mm according to the size and the geological nature of the site, some further concerns have to be tackled. Deformation might regard an entire portion of a slope or a limited region only. The former require to establish a stable ground reference system (GRS) to be held between different epochs, calling for the integration of high precision geodetic techniques; alternatively, a comparison with external stable areas is needed, but this solution usually does not guarantee enough accuracy. The latter might be solved for by considering relative displacements between close regions, for

example by adopting *Least Squares 3-D surface matching* (Acka, 2007 for theoretical and implementation aspects; Monserrat and Crosetto, 2008 for an application to landslides), or other locally adaptive method to compare DSMs (Digital Surface Models). In addition, vegetation can grow on the cliffs, introducing so that noise in observations and preventing from using the regions covered by bushes.

Secondly, boulders can fall down during observation epochs, resulting in significant changes on the surfaces. The evaluation of the amount and the spatial distribution of detachments is not only a prerequisite for the deformation analysis or a by-product of it, but it's a task that yields an important additional information, very useful to evaluate the real magnitude of rockfall process in a given area.

The measurement of the quantity of rocks detached from a cliff is a problem of *change detection* and will be the main subject of this paper. This application of TLS is expected to be really effective and to give an important contribute to the current practise. On the other hand, rock face deformation monitoring is a still open issue requiring further studies at theoretical and operational level.

In sections 2 and 3 some aspects concerning data acquisition and how to cope with georeferencing errors are presented by comparing results obtained from different approaches. In section 4 some techniques that can be applied for removing vegetation from point-clouds are presented and discussed, being this problem relevant when dealing with rock cliffs. All topics of the paper are referred to two cliffs located on the same mountain-side in the Italian Prealps. Results obtained from the application of the proposed techniques to both case studies are addressed in section 5.

## 2. DATA ACQUISITION

### 2.1 Test sites

Test sites are located on the same mountainside in the province of Lecco, northern Italy. The rock faces were chosen for their

geomorphological characteristics and for the proximity to a county road, as can be seen in Fig. 1. They are constituted by limestone (“Calcare di Esino”) characteristic of the Italian Prealps. In particular the rock face “B” presents a rock with many fractures and the effect of water, ice and thermal shock brought many small rock falls in the last years. Conversely, the rock face “A” presents a good and compact rock which didn’t result in recent rockfall events.

The rock face “A” (Fig. 2) features a morphology that is typical in the considered area. For this reason, it was chosen to evaluate the georeferencing problems in standard operational conditions. The mean distance from which scanning can be performed is large (160 m) and the placement of ground control points (GCPs) on the rock face surface was not possible due to its inaccessibility. The rock face covers a vertical area of extension 75 m in width and 30 m in height, resulting in a line-of-sight from the scanner stand point w.r.t. the orthogonal surface that is rotated up to 40 deg in both horizontal and vertical directions. The rock face “B” is located in the inferior part of the same mountainside (see figures 1 and 2). It was selected to investigate the problem of vegetation filtering from scans. The rock face “B” is smaller than “A” and presents an extensions of 25x15 m. Laser scans were acquired from a mean distance of 15 m. During this research 4 measurement campaigns for the cliff “A” and 3 for the cliff “B” were carried out between the months of November 2007 and March 2008.

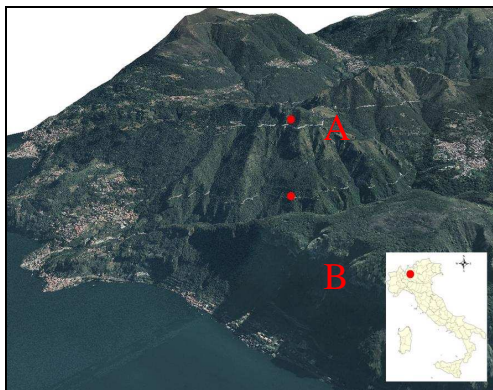


Figure 1.- Location of the rock faces (“A” and “B”) on the slopes of Mount Sasso di San Defendente in the Italian Prealps.



Figure 2.- Images of rock faces “A” (at top) and “B” (at bottom) where the red squares are the GCPs and the green circles are the independent check points.

## 2.2 Geodetic measurements

Geodetic measurements with a total station Leica Geosystems TCA 2003 (Leica, 2009) were performed at each observation epoch with a twofold aim.

The first one was to find the coordinates of GCPs to be used in the georeferencing process (only for cliff “B”). The GCPs consisted in square targets (side 5 cm) made of stainless steel plates covered by retro-reflective film, which is recognizable by both total station and TLS. Targets have been directly fixed on the rock surface.

The second aim was the validation of TLS monitoring measurements. Some benchmarks (ICHp, *independent check points*) were glued in the rock and during each geodetic measurement session a high-precision micro-prism was installed on them. Two more benchmarks outside of the cliff were placed for azimuth orientation. While on the test site “B” both types of targets (GCP and ICHp) were placed, on the test site “A” only GCPs outside of the cliff were used.

The stand-points setup for total station and TLS data acquisitions were materialized by a steel removable pillar, that could be installed on a plate and hooked up by a precise mechanical system. The plate was sunk into a concrete plinth of 50x50x25 cm. The installation sequence of the pillar is shown in Figure 3. When it was removed after the end of each measurement session, the basement could be completely hidden into the ground in order to reduce the environmental impact of the monitoring equipment and to allow its use also in parks and protected areas. The adopted pillar allowed the laser scanner repositioning on the same precise position at each time, and the TLS orientation was carried out by a mounting bracket. The georeferencing accuracy achieved by adopting GCPs, by *direct georeferencing* (Lichti and Gordon, 2004) and by both at the same time, will be compared and discussed in next section 3.

## 2.3 TLS data acquisition

The TLS data acquisition of the surface of rock face “A” was carried out using only one stand-point (station 100). Conversely, the rock face “B”, for its specific structure, has been surveyed from two different stand-points (200 and 300).



Figure 3.- Main steps of the installation of the TLS stand-point.

Use of the pillar enabled the coordinates of stand-points to be always fixed to the same position. To validate this hypothesis, geodetic measurements were repeated at each epoch. The use of a redundant scheme and the short distances involved allowed to obtain high precisions in 3D point determination (see the right-most columns in table 1). The relative displacements between consecutive epochs resulted in absolute value less than 1mm for all stand-points. In some cases, especially in  $z$  direction, displacements slightly larger than the corresponding standard deviations were found. These are probably due to small errors in the repositioning of micro-prisms.

The laser scanning survey has been carried out by a time-of-flight instrument Riegl LMS-Z420i. Technical information about it can be directly retrieved from the vendor website.

In all measurement sessions the same scanning parameters and acquisition windows were adopted (see table 2). In order to improve the precision, each scan was acquired in “multiscan” mode, i.e. it was repeated 4 times.

	Epoch	Stand point	$\Delta x$ [mm]	$\Delta y$ [mm]	$\Delta z$ [mm]	$\sigma_{xy}$ [mm]	$\sigma_z$ [mm]
Cliff “A”	Nov 07	100	-	-	-	$\pm 0.5$	$\pm 0.1$
	Dec 07	100	0.4	-0.3	-0.2	$\pm 0.6$	$\pm 0.1$
	Feb 08	100	-0.6	0.3	-0.4	$\pm 0.7$	$\pm 0.1$
	Mar 08	100	-0.7	0.0	0.5	$\pm 0.4$	$\pm 0.1$
	Mean	100	-0.3	0.0	0.0	$\pm 0.6$	$\pm 0.1$
Cliff “B”	Dec 07	200	-	-	-	$\pm 0.6$	$\pm 0.1$
		300	-	-	-	$\pm 0.6$	$\pm 0.1$
	Feb 08	200	-0.8	0.1	-0.2	$\pm 0.6$	$\pm 0.1$
		300	-0.2	0.0	0.2	$\pm 0.6$	$\pm 0.1$
	Mar 08	200	-0.8	0.0	-0.2	$\pm 0.5$	$\pm 0.1$
		300	-0.4	-0.2	0.6	$\pm 0.5$	$\pm 0.1$
	Mean	200	-0.8	0.0	-0.2	$\pm 0.5$	$\pm 0.1$
		300	-0.3	-0.1	0.4	$\pm 0.5$	$\pm 0.1$

Table 1.- Relative displacements of all TLS stand-points between consecutive measurement epochs. The right-most columns show the standard deviations of single-epoch measurements.

Scan		100	200	300
Scanning time [min]		74	42	43
# total measured points		19.99M	13.26M	13.74M
Angular resolutions [deg]	Horiz.	0.012	0.038	0.039
	Vert.	0.012	0.038	0.039
Mean grid resolution [m]	Min	0.03	0.01	0.01
	Max.	0.04	0.02	0.02
Acquisition range [m]	Min.	135	9	9
	Max.	202	23	26
Field-of-View [deg]	Horiz.	50.565	94.86	99.639
	Vert.	14.232	52.326	54.211
Laser beam spot-size [m]	Min.	0.034	0.002	0.002
	Max.	0.051	0.006	0.007

Table 2.- Parameters setup for scanning on the Riegl LMS-Z420i.

### 3. LASER SCAN GEOREFERENCING

For any monitoring operation the choice and materialization of a stable reference system is fundamental. Here a GRS was materialized by using the steel pillars and the GCPs. The first concept was to exploit the direct georeferencing of each TLS

stand-point, based on its repositioning on the pillar. Unfortunately, the docking system of TLS on the pillar failed to fix the horizontal rotation of the *instrumental reference system* (IRS), despite it was designed for this purpose. Then some other approaches have been tried and discussed in the following.

The method adopted to compare the different scans at two epochs  $t_i$  and  $t_{i+1}$  is the same presented in Alba *et al.* (2006). This consists in comparing a triangulated surface derived from the point-cloud taken at epoch  $t_i$ , with single points of the scan at epoch  $t_{i+1}$ . This method allows to compute only the displacements in the direction orthogonal to the surface at epoch  $t_i$ .

#### 3.1 Rock face “A”

In order to evaluate the quality of the repositioning, during the first epoch of measurement two different scans were captured from the same stand-point. These were used to validate the best georeferencing methods to adopt hereafter.

An overview of results obtained from different configurations is shown in table 3, whilst figure 4 reports some 2-D deformations maps computed by applying different parameter sets.

**3.1.1 Direct georeferencing (method A).** The docking system permits the direct georeferencing of the TLS on the pillar. However, this solution presented a large error in the horizontal rotation between IRS and GRS, as already described at the beginning of this section. The rotation error is estimate in  $\pm 0.1$ deg.

**3.1.2 Georeferencing by GCP (method B).** Scans have been georeferenced by using 5 GCPs. For the impossibility to reach the rock face, targets were not positioned on it, but in the nearby of the stand-point.

In the same way as we verified in other monitoring tests, with this method the required precision cannot be achieved, although the estimated transformation presents low residuals on GCPs (standard deviation  $\pm 2$  mm).

In order to improve the precision of georeferencing by GCPs, other algorithms to define the position of the target centre were tested (Alba *et al.*, 2008). However, no significant improvements were observed.

**3.1.3 IRS centre constrained and independent determination of rotations (methods C and D).** This method would like to overcome the limitation of method A in fixing the horizontal rotation. To do this, the rotation matrix of the roto-translation is calculated independently by using GCPs (method C) or by registering both point-clouds with an ICP (*Iterative Closest Point*, Besl and McKay, 1992) *surface matching algorithm* (method D).

In case of method C, results are similar to those achieved without the rigid constraint on shifts. In case of method D, a pre-alignment based on GCPs was carried out, and after the ICP algorithm was applied. This method allowed to sharply improve the relative precision of scan registration, and a RMSE=16 mm was obtained.

#### 3.2 Rock face “B”

In the cliff “B”, the alignment and georeferencing of the two scans were both simpler tasks. Thank to the possibility to put the targets directly on the rock face, the short range and the good overlap between the two adjacent scans, all methods described in Sec. 3.1 permitted to obtain good results, barring the direct georeferencing (method A).

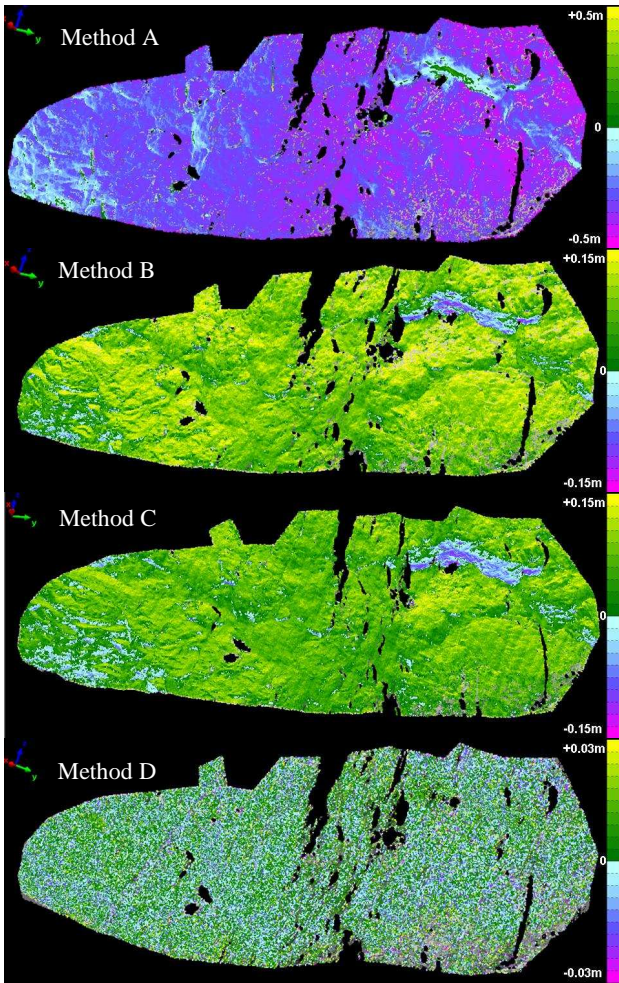


Figure 4.- Deformation maps evaluated by using different georeferencing methods applied to the cliff “A”.

Method	A	B	C	D
# points	701k	704k	709k	703K
Mean [mm]	253	83	77	1
Std.dev. [mm]	±110	±71	±79	±16
RMSE [mm]	275	109	110	16

Table 3.- Discrepancies along the orthogonal direction to the surface obtained from the application of different georeferencing methods to the cliff “A”

For these grounds, the method requiring less interaction (method 3) was chosen. The test on the scans acquired at the same epoch (Dec 07) gave the following result: mean of displacements 0.2 mm,  $\sigma = \pm 9.2$  mm, RMSE=9.2 mm. In Fig. 5 a 2-D map showing point displacements between point-clouds captured on the cliff “B” is reported. The evaluated deformations are not statistically significant.

#### 4. VEGETATION FILTERING

A recurrent problem occurring in rock slopes analysis is due to the presence of vegetated areas which prevent the acquisition of the bare cliff surface. In literature the problem of vegetation filtering is widely afforded on *airborne laser scanning* (ALS) data for Digital Terrain Model (DTM) reconstruction.

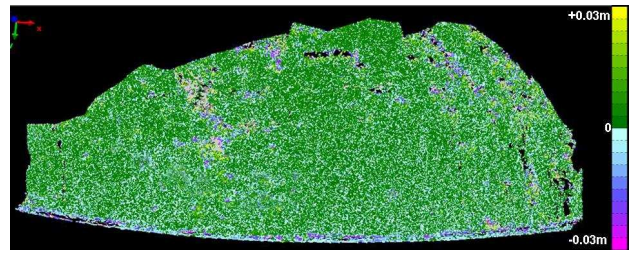


Figure 5.- Deformation map evaluated by using method C on the cliff “B”.

In this field, different methods have been proposed for removing the off-ground points. The principal difference between ALS and TLS is the possibility to measure for each impulse different echoes of the laser return. This fact obviously helps to identify the vegetation, especially trees. Only the latest generation of TLSs can carry out this task (see e.g. the Riegl VZ-400). The instrument used for this test does not feature this option, likewise all instruments adopted so far. On the other hand, the effectiveness of filtering data by using multi-echoes on terrestrial lasers is to be practically proved, because it depends on the size of laser spot and on that of holes in the vegetation mass.

Here the interest was focused on two *3D spatial filtering* techniques which exploit the redundancy in the point-cloud. These will be described (Subsec. 4.1) and applied to data of the test site “B” (Subsec. 4.2). Secondly, the possible use of an infrared camera combined to the laser scanning data is analysed (Subsec. 4.3).

Unfortunately, the unavailability of multi-echo data results in the fact that where the vegetation is recognized and filtered, the real rock surface cannot be reconstructed, but the corresponding areas are only labelled as no-data regions.

#### 4.1 3D spatial filters

**4.1.1 Octree filter.** This filter (Kilian *et al.*, 1996) is based on the reorganization of each point-cloud as an *octree* data structure. The whole volume enclosing the point-cloud is splitted into many small parallelepipeds, whose size is selected by the operator. Inside each elementary volume, the point showing the minimum value for one of the 3 coordinates (usually  $z$ ) is selected. indeed, the effectiveness of this method is based on the fact the  $z$  direction is roughly orthogonal to the rock surface. The quality of the filtering is function of the cell size: the bigger is the cell volume, the better is the probability to have a point on the rock, but with a low-pass filtering effect which is in a detriment of the model resolution.

**4.1.2 Iterative filtering.** This filter fits an interpolating surface to the data and accepts individual points in accordance with their distance to the surface (Axelsson, 2000). The filter generates a 2.5-D (DEM - Digital Elevation Model) surface from the unorganized raw point-cloud  $S$ . To do this task, in a given region of  $S$  a reference plane  $\pi_i$  is adopted, where a lattice made up of square cells is established. If the original point-cloud would feature a more complex shape, many reference planes will be adopted. The whole point-cloud  $S$  is then projected onto  $\pi_i$ ; if more than one point belongs to the same raster cell of size  $\Delta$ , only the point with  $z_{min}$  is selected, where the  $z$  axis is the orthogonal direction to  $\pi_i$ . After this initial stage, a sub-set  $S'$  of the full dataset  $S$  is selected. A regular grid DEM is derived from  $S'$ . Now  $S$  is compared to the DEM

surface and points closer than a threshold ( $d_{max}$ ) are kept. Then process is repeated iteratively by reducing at each step the size of both parameters  $\Delta$  and  $d_{max}$  until the vegetation is completely removed.

#### 4.2 Application to rock faces

The problem of the vegetation filtering on rock faces is more complex than usually it is with ALS data. First, bushes on a cliff grow in a direction that is quite parallel to that of the face itself, not orthogonal likewise trees on a flat terrain. This makes really difficult their automatic recognition. On the other hand, also the kind of vegetation growing on cliffs might influence the result of filtering; e.g. turf grass is hardly distinguishable from the background.

The problem of vegetation has been found only in the test site “B”, where however it is really relevant. There both methods in subsection 4.1 were applied.

The first stage of filtering, common to all methods, consisted in averaging the raw data captured in the “multiscan” modality. By fixing a threshold on the standard deviation of the ranges to be averaged, many areas with vegetation are filtered out. In figure 6 an image before and after the resampling by a threshold of 1.5 cm is shown, where it is evident that this operation can filter a large part of the vegetation on the cliff.

Then the resampled dataset was filtered by both methods described in subsections 4.1 and 4.2.

The *octree filter* enabled to remove the vegetation only if large size cells were adopted, with consequent drop of spatial resolution. The *iterative method* enabled to remove the most vegetation but to preserve a dense point-cloud. Drawbacks of this method is that it is not capable to take apart the vegetation from overhang and nook which are on the cliff, and consequently they are removed as well. For this reason it is essential a manual check of the eliminated points (see Fig. 7).

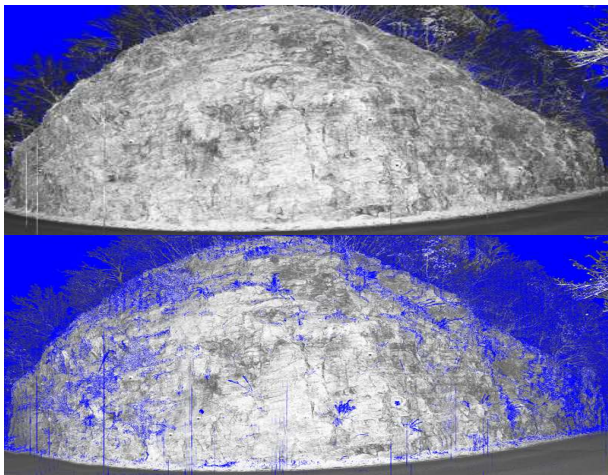


Figure 6.- Intensity images of the point-cloud of the rock face “B” before (at top) and after (at bottom) the resampling of “multiscan” data.

#### 4.3 Integration of infrared imagery

Because of the morphological complexity of a rock face, it is very difficult to obtain satisfactory results with semi-automated spatial filters like those described in subsection 4.1. For this reason, a new automatic system able to identify the vegetation

has been designed. The use of a high resolution *near infrared camera* allows to recognize the vegetation with high accuracy. Figure 8 shows an image with IR channel at wavelength 730 nm (red parts are mainly plants containing chlorophyll) of a cliff, very similar to that at issue, captured by a hyperspectral camera HySpex.

TLS integrating an infrared camera is probably capable to resolve the problem with easy and to provide an accurate fully automatic filtering.

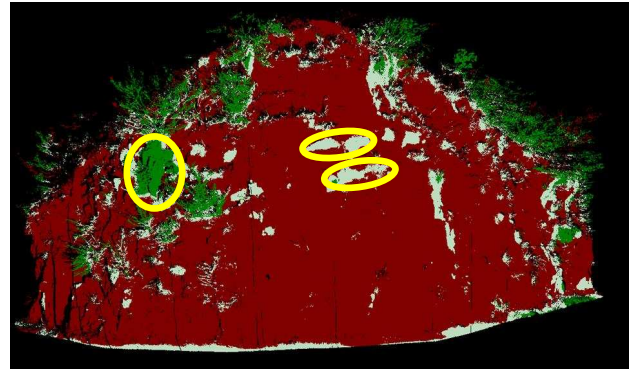


Figure 7.- Filtering data by *iterative method*: the dark green areas represent the point filtered out after the first step, the light green areas the ones after the second step, while the yellow ellipses represents manual error editings.

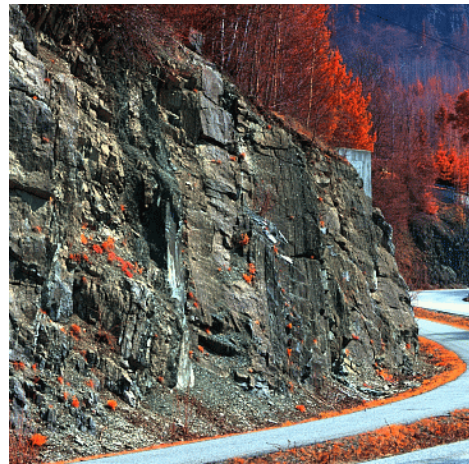


Figure 8.- Image showing an artificial RGB image with red channel at 730nm (red parts are mainly plants containing chlorophyll).

### 5. CHANGE DETECTION RESULTS

In order to check out possible deformations and to find areas where rock detachments occurred, the laser scans taken at different epochs were compared. At each epoch the same data acquisition and processing pipeline (see sections 2, 3, 4) were applied. The method for the pairwise comparison of scans that has been addressed at Sec. 3 was used.

The cliff “A” didn’t show marks of deformation or rockfalls like it can be seen in figure 9 (at top), which shows the full displacements between the first and last epochs. The displacements are normally distributed on the entire surface and

the 95% of points are included in a range of  $\pm 2$  cm, which corresponds to the precision of the adopted TLS (see table 4). Displacements found here are not statistically significant. In the rock face “B” a little change has been observed in each epoch. In figure 9 (at bottom) only the negative displacements (corresponding to rock losses and not to grown vegetation) larger than 2 cm are represented in order not to show significant displacements only. The red rectangles show some zones of rock fall; some of these were also validated by the presence of the corresponding rock fragments on the adjacent road. In other areas the comparison between the data highlighted other possible rockfalls, but these could be due to the change in volume of the vegetation that had not been properly filtered out. These areas can be identified by looking at the map of positive errors. By comparing the data there are clear admissions of new cavities that were not present on the cliff during the first scan. These are significant in size, with an estimated depth up to a few centimetres.

	Epoch $t_i$	Nov 07	Dec 07	Feb 08
	Epoch $t_{i+1}$	Dec 07	Feb 08	Mar 08
Cliff “A”	# points	702k	705k	704k
	Mean [mm]	-1	-1	0
	Std.dev. [mm]	11	11	11
	RMSE [mm]	11	11	11
Cliff “B”	# points	-	179K	175K
	Mean [mm]	-	0	3
	Std.dev. [mm]	-	9	10
	RMSE [mm]	-	9	10

Table 4.- Monitoring results on rock faces “A” and “B” at each epoch, in term of displacements in normal direction to the rock surface.

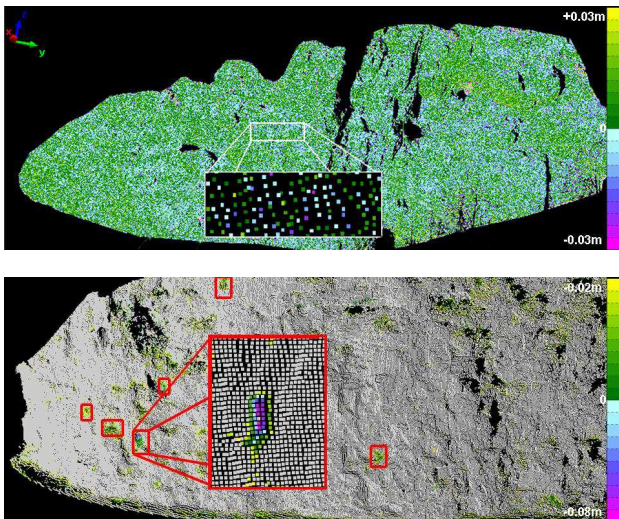


Figure 9.- Deformation map between the first and the last epochs of the full rock face “A” (at top) and “B” (at bottom); in the case of cliff “B”, only the negative significant displacements larger than 2 cm are shown.

## 6. CONCLUSIONS

The presented methodology has been allowed us to reconstruct with high precision the shape of the cliff in order to identify and

assess the areas and the extent of the detachments occurred even for small collapses of rock (a few cube centimetres).

In this paper two particular aspect have been analysed, the problem of scan georeferencing and the filtering of vegetation. In particular, the former has been tackled by the integrated use of a physical constraint to the shifts of the instrumental reference system and of an ICP algorithm to solve for rotations (or alternatively the only use of GCPs in case of a short acquisition distance). The problem of vegetation filtering has been addressed by two methods which have given fairly good results but that have been rather laborious to be applied. For this reason, a new method based on infrared images integrated to a TLS instrument has been proposed.

## REFERENCES:

Abellán, A., Vilaplana, J. M., and J. Martínez, 2006. Application of a long-range terrestrial laser scanner to a detailed rockfall study at Vall de Núria, *Eng. Geol.*, 88(3-4), pp. 136-148.

Acka, D., 2007. Matching of 3D Surfaces and their intensities. *ISPRS J. Photogramm. Remote Sens.*, 62(2), pp. 112-121.

Alba, M., Fregonese, L., Giussani, A., Prandi, F., Roncoroni, F., Scaioni, M., and P. Valgoi, 2006. Structural Monitoring of a Large Dam by Terrestrial Laser Scanning. In: *IAPRSSIS*, Dresden, Germany, Vol. XXXVI, Part 5, pp. 6, on CDROM.

Alba, M., Roncoroni, F., and M. Scaioni, 2008. Investigations about the accuracy of target measurement for deformation monitoring. In: *IAPRSSIS*, Beijing, China, Vol. XXXVII, Part B5, pp.1053-1060.

Axelsson P., 2000. DEM generation form Laser Scanner Datausing adaptive TIN Models. In: *IAPRSSIS*, Amsterdam, the Netherlands, Vol. XXXIII, Part B4/1, pp. 110-117.

Arosio, D., Longoni, L., Papini, M., Scaioni, M., Zanzi, L., and M. Alba, 2009. Towards rockfall forecasting through observing deformations and listening to microseismic emissions. Accepted for publication on *Nat. Hazards Earth Syst. Sci.*, pp. 13.

Besl, P.J., and N.D. McKay, 1992. A Method for Registration of 3D Shapes. *IEEE Trans. Pattern Anal. Mach. Intell.*, 14(2), pp. 239-256.

HySpex product and service. <http://www.neo.no/products/hyperspectral.html> (accessed on 6 Apr 2008).

Kilian, J., Haala, N., and M. Englich, 1996. Capture and evaluation of airborne laser scanner data. In: *IAPRS*, Vienna, Austria, Vol. XXXI, Part B3, pp. 383-388.

Leica. <http://www.leica-geosystems.com>, (accessed on 16 Jun 2009).

Lichti, D.D., and S.J. Gordon, 2004. Error Propagation in Directly Georeferenced Terrestrial Laser Scanner Point Clouds for Cultural Heritage Recording. In: Proc. of FIG Working Week, Athens, Greece, May 22-27, pp. 16, on CDROM.

Lindenbergh, R., and N. Pfeifer, 2005. A statistical deformation analysis of two epochs of terrestrial laser data of a lock. In: Proc. Of 7th Optical 3-D Measurement Techniques, Vienna, Austria, 3-5 Oct, Part 2, pp. 61-70.

Monserrat, O., and M. Crosetto, 2008. Deformation measurement using terrestrial laser scanning data and least squares 3D surface matching. *ISPRS J. Photogramm. Remote Sens.*, 63(1), pp. 142-154.

Roncella, R., and G. Forlani, 2005. Extraction of planar patches from point clouds to retrieve dip and dip direction of rock discontinuities. In: *IAPRSSIS*, Enschede, the Netherlands Vol. XXXVI, Part 3/W19, pp. 162-167.

Riegl. <http://www.riegl.com> (accessed on 16 Jun 2009).

Schneider, D., 2006. Terrestrial laser scanner for area based deformation analysis of towers and water damns. In: Proc. of 3<sup>rd</sup> IAG Symp., Baden, Austria, 22-24 May, pp. 6, on CDROM.